Research Article Vol. 5, No. 6 / June 2018 / Optica 718

Experimental test of quantum correlations from Platonic graphs

Ya Xiao,[1,2,†] Zhen-Peng Xu,[3,4,†] Qiang Li,[1,2] Hong-Yi Su,[5] Kai Sun,[1,2] Adán Cabello,[4] Jin-Shi Xu,[1,2,7] Jing-Ling Chen,[3,6,8] Chuan-Feng Li,[1,2,9] and Guang-Can Guo[1,2]

[1]CAS Key Laboratory of Quantum Information, University of Science and Technology of China, Hefei 230026, China
[2]Synergetic Innovation Center of Quantum Information and Quantum Physics, University of Science and Technology of China, Hefei 230026, China
[3]Theoretical Physics Division, Chern Institute of Mathematics, Nankai University, Tianjin 30071, China
[4]Departamento de Fisica Aplicada II, Universidad de Sevilla, E-41012 Sevilla, Spain
[5]Graduate School of China Academy of Engineering Physics, Beijing 100193, China
[6]Centre for Quantum Technologies, National University of Singapore, 3 Science Drive 2, Singapore 117543, Singapore
[7]e-mail: jsxu@ustc.edu.cn
[8]e-mail: chenjl@nankai.edu.cn
[9]e-mail: cfli@ustc.edu.cn

Received 29 January 2018; revised 23 April 2018; accepted 7 May 2018 (Doc. ID 320891); published 29 May 2018

Great effort has been made in the investigation of contextual correlations between compatible observables due to their both fundamental and practical importance. The graph-theoretic approach to correlate events has been proved to be an effective method in the characterization of quantum contextuality, which implies that quantum violations of noncontextual inequalities derived in the noncontextual hidden-variable models should be achievable. Finding experimentally more friendly and theoretically more powerful noncontextual inequalities associated with specific graphs is of particular interest. Here we consider Platonic graphs to vindicate the quantum maximum predicted by graph theory and test the quantum violation against the mixedness of the state. Among these solids we refer particularly to the icosahedron to build the experiment, as it gives rise to the largest quantum-classical difference. The contextual correlations are demonstrated on quantum four-dimensional states encoded in the spatial modes of single photons generated from a defect in a bulk silicon carbide. Our results shed new light on the conflict between quantum and classical physics and may promote deep understanding of the connection between quantum theory, graph theory, and operator theory.

OCIS codes: (270.0270) Quantum optics; (270.5585) Quantum information and processing; (000.2190) Experimental physics.

https://doi.org/10.1364/OPTICA.5.000718

1. INTRODUCTION

As basic mathematical objects, graphs have been studied extensively, for they not only demonstrate purely scientific aesthetics but also have many important applications in all branches of science. Very recently, Cabello *et al.* [1] have discovered that there is a fundamental connection between graphs and the contextual correlations between the outcomes of compatible experiments on quantum systems (i.e., *contextuality* [2,3]). For any graph one can imagine, there exist a quantum system and a set of projective measurements producing "events"—characterized by the outcomes of a set of compatible projective measurements—which are in one-to-one correspondence with the vertices of the graph, such that whenever there is an edge between the vertices, any pair of these events correspondingly are exclusive (i.e., cannot happen at the same time, or can be distinguished by a projective measurement) [4,5]. More precisely, the central idea of the graph-theoretic approach to quantum correlations is that an arbitrary N-vertex graph can always be associated with a noncontextuality inequality (NC inequality):

$$S = \sum_{i=1}^{N} \langle \hat{P}_i \rangle \leq \alpha, \tag{1}$$

where $\langle \hat{P}_i \rangle$ is the projective probability of the rank-one projector $\hat{P}_i$ corresponding to the ith vertex in the graph, and α is the independence number of the graph [6]. All noncontextual hidden-variable (NCHV) models satisfy Inequality (1), but quantum mechanics (QM) can beat the classical bound α, thus revealing the contextual correlations. As described in [7], the logical Bell inequalities of Abramsky and Hardy (building on the framework of Abramsky–Brandenburger [8]) can also be investigated in a similar way.

In fact, the sum of the physically possible probabilities of these events necessarily corresponds to a point of the Grötschel–Lovász–Schrijver theta body of the graph, the latter being a set

of purely combinatorial objects [9]. In particular, the maximum value of the sum is exactly the Lovász number (usually denoted by ϑ) of the graph, which was originally introduced as an easy-to-approximate number between two hard-to-approximate numbers in graph theory [10]. Such a correspondence between graphs and quantum-correlation experiments is remarkable, as it (i) places some bound on the quantum set [11], (ii) suggests that correlations in nature are essentially bounded by a simple physical principle (the exclusivity principle [12–14]) valid in all scenarios, instead of the ones only applied within Bell's scenario, and (iii) has been a key to explore quantum supremacy in quantum computation [15–18]. The correspondence has thus far been proved useful to write out interesting forms of contextual correlation through a series of work [19–25].

In this work, we develop the exact forms of contextual relations from Platonic graphs. By strictly measuring the contextual correlations between compatible observables on quantum four-dimensional states encoded in the spatial modes of single photons generated from a defect in a bulk silicon carbide, we experimentally demonstrate the quantum contextuality of the icosahedron graph, which gives rise to the largest quantum-classical difference.

2. THEORETICAL FRAMEWORK

We start with graphs associated with Platonic solids, or to shorten it, Platonic graphs, i.e., the five graphs that have each of the five Platonic solids as skeletons. The details can be found in Sections 1 and 2 in Supplement 1. To have the Platonic graphs tested in a quantum-correlation experiment with the satisfactory compatibility requirements, we adopt the following alternative NC inequality [26]:

$$S = \sum_{i\in V} P_{|\psi\rangle}(A_i = 1) - \sum_{(A_i,A_j)\in E} P_{|\psi\rangle}(A_i = 1, A_j = 1) \overset{\text{NCHV}}{\leq} \alpha(G) \overset{\text{QM}}{\leq} \vartheta(G), \tag{2}$$

where V and E, respectively, denote the vertex and edge sets of the graph $G(V,E)$, $P_{|\psi\rangle}(A_i = 1)$ denotes the probability of obtaining result 1 when the observable $|A_i\rangle\langle A_i|$ is measured on the state $|\psi\rangle$. Inequality (2) is deviated from Inequality (1) by adding the second term, which contains the joint probabilities $P_{|\psi\rangle}(A_i = 1, A_j = 1)$ $(= P_{|\psi\rangle}(A_i = 1)P_{|A_i\rangle}(A_j = 1))$ that represent experimental imprecision when $|A_i\rangle$ and $|A_j\rangle$ are measured successively. A remarkable point is that these two inequalities share the same classical bound and the same quantum violation, but the latter is convenient for analyzing the compatibility conditions. The introduction of the second term into Inequality (2) is crucial and necessary: it is important to evaluate the two-point probability $P_{|\psi\rangle}(A_i = 1, A_j = 1)$ in order to fulfill the compatibility requirement in any contextuality test [26].

In this work, we choose to experimentally test contextual correlations from the icosahedron graph as shown in Fig. 1. The reasons are threefold. (i) Among the five Platonic graphs, the ratio of the quantum violation (ϑ) to the classical bound (α) is maximal for the icosahedron graph. The larger the ratio, the more friendly the experimental observation. (ii) To our knowledge, the ratio ϑ/α of the icosahedron graph is maximal for all graphs that we have known, at least for all regular polyhedrons in any dimension (including all regular polygons in two dimensions). (iii) For the icosahedron graph, almost all four-dimensional states (except the maximally mixed state) violate the NC inequality, thus one can

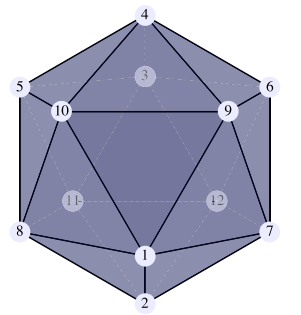

(a)

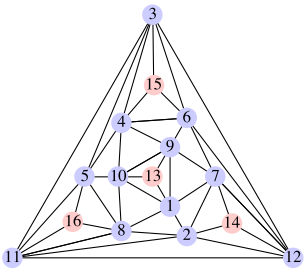

(b)

$\|1\rangle$	τ	0	$-\phi$	1
$\|2\rangle$	τ	0	ϕ	1
$\|3\rangle$	τ	0	ϕ	-1
$\|4\rangle$	τ	0	$-\phi$	-1
$\|5\rangle$	τ	1	0	ϕ
$\|6\rangle$	τ	-1	0	ϕ
$\|7\rangle$	τ	-1	0	$-\phi$
$\|8\rangle$	τ	1	0	$-\phi$
$\|9\rangle$	τ	ϕ	1	0
$\|10\rangle$	τ	$-\phi$	1	0
$\|11\rangle$	τ	$-\phi$	-1	0
$\|12\rangle$	τ	ϕ	-1	0
$\|13\rangle$	ϕ'	0	$-\tau'$	$-\omega$
$\|14\rangle$	ϕ'	$-\tau$	$-\tau$	τ
$\|15\rangle$	ϕ'	ω	0	τ'
$\|16\rangle$	ϕ'	$-\tau'$	ω	0
$\|\psi\rangle$	1	0	0	0

(c)

α	ϑ	ϑ/α
3	$3(\sqrt{5}-1)$	1.236

(d)

Fig. 1. Icosahedron graph. (a) The icosahedron solid with 12 vertices. (b) The 12 blue vertices depict the corresponding icosahedron graph. Four red vertices are added for the need of experimental test for the compatibility conditions. (c) The corresponding optimal quantum initial state $|\psi\rangle$ and measurement settings $|i\rangle$. The set $\{|1\rangle, |2\rangle, \ldots, |12\rangle\}$ forms the Lovász optimum orthogonal realization. $|i\rangle$ (unnormalized vector for simplicity) denotes $|A_i\rangle$. $\tau = \sqrt{\phi}$, $\phi = \frac{1}{2}(\sqrt{5}+1)$, $\tau' = 1/\tau$, $\phi' = 1/\phi$, $\omega = \sqrt{2+\sqrt{5}}$, and $\sum_{i=1}^{12} |\langle\psi|A_i\rangle|^2 = 3(\sqrt{5}-1)$ give the quantum maximum that equals to the Lovász number. (d) The independence number α and the Lovász number ϑ of the icosahedron.

reveal the contextuality for almost all four-dimensional states by a single inequality. To a certain sense, such an experimental revealing has merit over the state-independent contextuality proof with 18 rays [27,28], because experimentally the former requires fewer projective measurements but with larger quantum violations.

Explicitly, we shall test the NC inequality corresponding to the icosahedron graph as follows:

$$S = \sum_{i=1}^{12} P_{|\psi\rangle}(A_i = 1) - \sum_{(i,j)\in E} P_{|\psi\rangle}(A_i = 1, A_j = 1) \overset{\text{NCHV}}{\leq} 3. \tag{3}$$

Analytically, the quantum maximum can be proved equal to its corresponding Lovász number, with $S_{\text{QM}}^{\max} = \vartheta = 3(\sqrt{5}-1) \approx 3.708$. Moreover, it can be directly proved that all four-dimensional states except the maximally mixed state violate the single inequality. To have a simple proof, one can refer to the 4-vectors (i.e., the Lovász optimum orthogonal realization) and the initial state listed in Fig. 1(c). Ideally, the second summation terms in Inequality (3) vanish, so it suffices to consider the quantity $\sum_{i=1}^{12} |A_i\rangle\langle A_i|$, whose eigenvalues are $\{3(\sqrt{5}-1), 5-\sqrt{5}\}$, with the first one being the Lovász number and the last one threefold degenerate. With the maximally mixed state $\mathbb{1}/4$ as the least case, one can have $\frac{1}{4}[3(\sqrt{5}-1) + 3\times(5-\sqrt{5})] = 3$. Hence, any other states will violate the inequality.

Because the quantum system we utilize in experiment is four dimensional, we further extend the graph with extra projectors, A_{13}, A_{14}, A_{15}, and A_{16}, to construct *full* sets of compatible observables, such that every projector is measured as part of a complete basis [26]. In summary, the sets of observables are $\{A_1, A_9, A_{10}, A_{13}\}$, $\{A_2, A_7, A_{12}, A_{14}\}$, $\{A_3, A_4, A_6, A_{15}\}$, and $\{A_5, A_8, A_{11}, A_{16}\}$. The method to obtain detailed forms of the vectors can be found in Section 2 in Supplement 1. Each of the measurements can then be performed in the same orthogonal basis. The detection probability of each observable such as A_1 can be obtained as $P_{|\psi\rangle}(A_1 = 1) = \frac{N_{|\psi\rangle}(A_1)}{N_{|\psi\rangle}(A_1)+N_{|\psi\rangle}(A_9)+N_{|\psi\rangle}(A_{10})+N_{|\psi\rangle}(A_{13})}$, where $N_{|\psi\rangle}(A_i)$ is the number of counts of obtaining result 1 when the observable $|A_i\rangle\langle A_i|$ is measured on the state $|\psi\rangle$. Then, by measuring the contextual correlations between compatible observables on quantum four-dimensional states encoded in the spatial modes of single photons generated from a defect in a bulk silicon carbide, we observe the experimental proof-of-principle of this result.

3. EXPERIMENTAL SETUP AND RESULTS

Figure 2 shows our experimental setup. The information is encoded into the four spatial modes of a single photon. Single photons are generated by exciting an intrinsic defect (carbon antisite-vacancy pair) in a bulk high-purity semi-insulating 4H silicon carbide (SiC) [29]. The carbon antisite-vacancy pair defects in silicon carbides have been shown to be ultrabright, photostable single-photon sources even at room temperature. To match the operation wavelength of the half-wave plates in the contextuality test setup, we used a bandpass filter with a central wavelength of 720 nm and a width of 13 nm to filter the fluorescence of the defects. The total photon count for each set of measurement is about 40,000. The second-order photon correlation function at zero delay without background correction is $g^2(0) = 0.268$ (with the fitting to 0.04), which clearly shows the signature of photon antibunching [the inset in Fig. 2(a)].

The single photon is then directed to the contextuality test setup constructed by several half-wave plates (HWPs) and beam displacers (BDs). A beam displacer is a birefringent crystal, in which light beams with horizontal and vertical polarizations are separated by a certain displacement. The polarization of the photon can be rotated using half-wave plates, and the relative amplitudes of different spatial modes can be conveniently adjusted.

The polarization of the single photon initially in the spatial modes i_1 is first rotated by HWP1, which is horizontally separated into i_1 and i_3 after the first beam displacer. The two half-wave plates (HWP2 and HWP3) further rotate the polarizations of the photon in the corresponding spatial modes, which are vertically separated by the second beam displacer. The final state we prepared can be the superposition of four spatial modes i_1, i_2, i_3, and i_4. The amplitudes of the four spatial modes can be changed by adjusting the angles of the HWP1, HWP2, and HWP3. To prepare a diagonal mixed state, three glasses with different lengths are inserted into paths $|i_1\rangle$, $|i_2\rangle$, and $|i_3\rangle$ (not shown in Fig. 2) to completely destroy the coherence between spatial modes. We build different kinds of measurement settings. Three of them are shown in Fig. 2, i.e., the projection to the superposition states of spatial modes of i_1, i_2, and i_3 [$1 + 2 + 3$, Fig. 2(b)], the projection to i_1, i_2, and i_4 [$1 + 2 + 4$, Fig. 2(c)] and to i_1, i_3, and i_4 [$1 + 3 + 4$, Fig. 2(d)]. There, the quantum information encoded in spatial modes is converted back into polarization-encoded quantum information. The angle of HWP4 is set to be 45° such that the paths i_1 and i_3 (i_2 and i_4) are combined to one path after the third beam displacer. The unwanted path in the corresponding measurement is denoted by the dashed line. The relative amplitudes of the

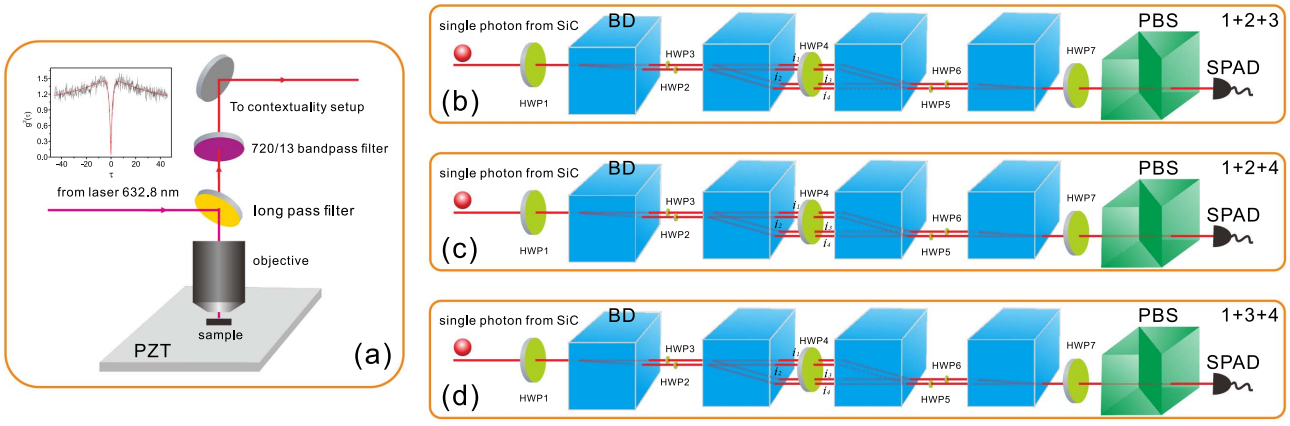

Fig. 2. Experimental setup. (a) The individual system (single photon) is prepared by exciting an intrinsic defect, known as the carbon antisite-vacancy pair in a bulk SiC sample. The insert shows the second-order photon correlation function of the emitting photons. $g^2(0) = 0.268$ (with the fitting to 0.04) clearly confirms the character of single-photon emission. The emitted single photon is filtered by a bandpass filter with a central wavelength of 720 nm and a bandwidth of 13 nm, and is sent to the contextuality test setup. (b)–(d) show the contextuality test setup with the same initial state preparation setup and different final measurement settings. The four-dimension states are encoded into the spatial modes of the single photon (i_1, i_2, i_3, and i_4), which are prepared by passing the photon through the half-wave plate 1 (HWP1), and two beam displacers (BDs) with two more half-wave plates (HWP2 and HWP3) in each of the spatial modes. To prepare a mixed state, three glasses with different lengths are inserted into paths $|i_1\rangle$, $|i_2\rangle$, and $|i_3\rangle$ (not shown in the figure) to completely destroy the coherence between different spatial modes. Three kinds of projective measurement settings with four half-wave plates (HWP4, HWP5, HWP6, and HWP7) and two BDs are employed, i.e., (b) the projection to the superposition states with spatial modes of 1, 2, and 3 ($1 + 2 + 3$), (c) the projection to the superposition states with spatial modes of 1, 2, and 4 ($1 + 2 + 4$) and (d) to the superposition states of spatial modes with 1, 3, and 4 ($1 + 3 + 4$). The polarization is finally selected by a polarization beam splitter (PBS) and the photon is detected by a single photon avalanche photodiode (SPAD).

projected state can be adjusted by the last three half-wave plates, i.e., HWP5, HWP6, and HWP7. The polarization of the photon is finally rotated to be horizontal which is determined by a polarization beam splitter (PBS), and the photon is detected by a single photon avalanche photodiode (SPAD).

To test Inequality (3), we need to check the contextuality between two successive measurements. As proposed in Ref. [26], the statistics of the second measurements affected by the first measurements can be calculated as

$$\varepsilon(\_,0|\_,A_j) = |P_{|\psi\rangle}(A_j=0) - \sum_{k=0}^{1} P_{|\psi\rangle}(A_i=k, A_j=0)|,$$

$$\varepsilon(\_,1|\_,A_j) = |P_{|\psi\rangle}(A_j=1) - \sum_{k=0}^{1} P_{|\psi\rangle}(A_i=k, A_j=1)|,$$

and similarly for $\varepsilon(0,\_|A_i,\_)$ and $\varepsilon(1,\_|A_i,\_)$, which represent the statistics of the first measurements affected by the second measurements. We need to check that, within the experimental precision, the influence of the first measurements on the second ones is as negligible as the influence of the second measurements on the first ones whenever $\varepsilon(\_,0|\_,A_j) \approx \varepsilon(0,\_|A_i,\_)$ and $\varepsilon(\_,1|\_,A_j) \approx \varepsilon(1,\_|A_i,\_)$. To obtain $P_{|\psi\rangle}(A_i=0,A_j=1)$ $(= P_{|\psi\rangle}(A_i=0)P_{|A_i^{\perp}\rangle}(A_j=1))$, we need to prepare $|A_i^{\perp}\rangle$, which represents the remained state after a projective measurement of $|A_i\rangle\langle A_i|$ on the initial state $|\psi\rangle$ with the outcome 0. The process is realized by the blocking method. We express the state $|\psi\rangle$ in a complete orthogonal basis $\{A_i, A_{i'}, A_{i''}, A_{i'''}\}$. By blocking $|A_i\rangle$, the remaining state turns to be $|A_i^{\perp}\rangle$, which is further projected to $|A_j\rangle$ with the outcome 1. The measurement setup is the same as that of Fig. 2. We further clarify detailed methods to measure the statistics between successive measurements in Section 3 in Supplement 1.

In our experiment, the input state is prepared as

$$\rho = a|i_1\rangle\langle i_1| + b|i_2\rangle\langle i_2| + c|i_3\rangle\langle i_3| + d|i_4\rangle\langle i_4|, \quad (4)$$

with a, b, c, and d representing the corresponding amplitudes in the components of $|i_1\rangle\langle i_1|$, $|i_2\rangle\langle i_2|$, $|i_3\rangle\langle i_3|$, and $|i_4\rangle\langle i_4|$, respectively. $\{|i_1\rangle, |i_2\rangle, |i_3\rangle, |i_4\rangle\}$ forms an orthogonal basis for the four-dimensional space, and $a+b+c+d=1$. We denote the state as $\mathrm{Diag}(a,b,c,d)$.

To verify Inequality (3), we need to check the measurement statistical effect for the state ρ. Because ρ is classically mixed by four orthogonal bases, the corresponding probabilities of the four bases can be experimentally measured by counting photons in each path. We test the statistical effect when the four bases of $|i_1\rangle$, $|i_2\rangle$, $|i_3\rangle$, and $|i_4\rangle$ are used as the input states. The experimental results of the measurement statistical effect are shown in Section 4 in Supplement 1. For the four input states, one can have $\varepsilon(\_,0|\_,A_j) \approx \varepsilon(0,\_|A_i,\_)$ and $\varepsilon(\_,1|\_,A_j) \approx \varepsilon(1,\_|A_i,\_)$ within the experimental precision. Error bars are calculated from the counting statistics.

Figure 3 further show the detailed probabilities for the input state of $|i_1\rangle$. Red dots represent the detection probabilities of the corresponding measurement settings of $P_{|i_1\rangle}(A_i=1)$ $(i \in \{1,12\})$ with the theoretical prediction of 0.309. To show the experimental precision in preparing two orthogonal states, the sum orthogonal probability of A_1 is defined as $P(A_1\perp) = P(A_1=1,A_2=1) + P(A_1=1,A_7=1) + P(A_1=1,A_8=1) + P(A_1=1,A_9=1) + P(A_1=1,A_{10}=1)$. The other eleven probabilities can be defined in the same way. In the experiment, the

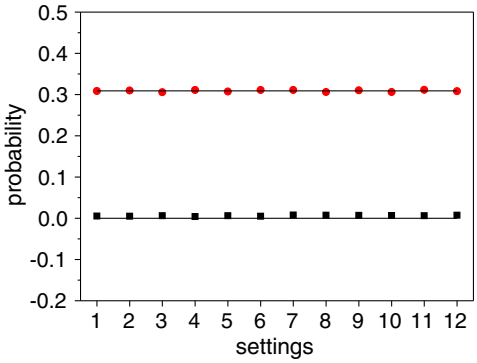

Fig. 3. Probabilities for the input state $|i_1\rangle$. Red dots represent the detection probabilities of the corresponding measurement settings of $P_{|i_1\rangle}(A_i=1)$ $(i \in \{1,12\})$ with the theoretical prediction of 0.309. Black squares represent the probabilities of $P(A_1\perp)$ to $P(A_{12}\perp)$, with the solid line representing the theoretical prediction of 0, which indicates the compatibility requirements are satisfied. The error bars deduced from the Poisson photon distribution are smaller than the symbols and cannot be seen clearly in the figure.

implementation of the projective measurement and the joint probability measurement correspond to detect the probabilities of the photon in several bases with different prepared states. The detailed method to calculate the probabilities can be found in Section 4 in Supplement 1. Black squares in Fig. 3 show the corresponding experimental results with the solid line representing the theoretical prediction of 0. As one has expected, for the pure input state, the summation of the 12 probabilities $P(A_i)$s approximately recover the Lovász number, thus coinciding with the theoretical prediction. The fluctuation of the polarization of background light in the imperfect single photon emission would affect the measurement result, which is shown to be small in our experiment.

Furthermore, we experimentally demonstrate that all four-dimensional states except the maximally mixed state violate single Inequality (3). To reach the purpose, we prepare four kinds of initial states, which are $\rho_1 = \mathrm{Diag}(x,y,0,0)$, $\rho_2 = \mathrm{Diag}(x,x,y,0)$,

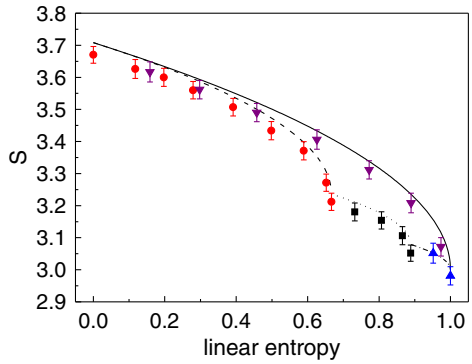

Fig. 4. Experimental results for the contextuality test. Red dots, black squares, blue upward triangles, and purple downward triangles represent the experimental results with the initial input states of $\rho_1 = \mathrm{Diag}(x,y,0,0)$, $\rho_2 = \mathrm{Diag}(x,x,y,0)$, $\rho_3 = \mathrm{Diag}(x,x,x,y)$, and $\rho_4 = \mathrm{Diag}(x,y,y,y)$ $(x \geq y)$, respectively. The dashed line, dotted line, dashed–dotted line, and solid line represent the corresponding theoretical predictions (only for the maximally mixed state $\mathrm{Diag}(1,1,1,1)/4$ is Inequality (3) not violated). Error bars are deduced from the Poisson photon distribution.

$\rho_3 = \mathrm{Diag}(x, x, x, y)$, and $\rho_4 = \mathrm{Diag}(x, y, y, y)$, here x and y represent the corresponding amplitudes and $x \geq y$. Figure 4 indicates that the experimental results coincide with our theoretical predictions. The x axis represents the linear entropy of the states, which is calculated as $\ell = 4(1 - \mathrm{Tr}(\rho^2))/3$. In particular, for the pure input state of $|i_1\rangle$ ($x = 1$ and $y = 0$), the value of S we obtained is $S = 3.671 \pm 0.026$, which violated NCHV prediction 3 by about 25 standard deviations.

4. DISCUSSION

It has been shown [23] that only about one-third of the quantum states of a three-dimensional system can be revealed by the simplest Klyachko–Can–Binicioğlu–Shumovsky inequality [30], which contains merely five measurements. Such kind of contextual correlation related to the simplest graph, pentagon, has been experimentally demonstrated by encoding a qutrit state (three-state system) into the path information of a trigger single photon [31]. However, Inequality (3) can detect almost all quantum states of a four-dimensional system. This fact reflects that different graphs have different powers to demonstrate contextual correlations. In our work, we have selected the icosahedron graph to test contextuality. Our quantum-correlation experiment sheds new light on the conflict between quantum and classical physics. Our results open a way for exploring quantum properties with graphs as a starting point and indicate that graph theory presents more physics than precedented thoughts.

Funding. National Key Research and Development Program of China (NKRDPC) (2016YFA0302700, 2017YFA0304100); National Natural Science Foundation of China (NSFC) (11325419, 11774335, 61327901, 61725504, 11475089); Fundamental Research Funds for the Central Universities (FRFCU) (WK2470000026, WK2470000020); Anhui Initiative in Quantum Information Technologies (AIQIT) (AHY060300, AHY020100); Key Research Program of Frontier Sciences (KRPFS), Chinese Academy of Sciences (CAS) (QYZDYSSW-SLH003); Ministerio de Economía y Competitividad (MINECO) (FIS2014-60843-P); "Advanced Quantum Information" (MINECO, Spain); European Regional Development Fund (ERDF); "Photonic Quantum Information" Knut och Alice Wallenbergs Stiftelse, Sweden.

Acknowledgment. J. L. Chen was supported by the National Natural Science Foundation of China. A. Cabello was supported by Project "Advanced Quantum Information" (MINECO, Spain), with FEDER funds and the project "Photonic Quantum Information" (Knut and Alice Wallenberg Foundation, Sweden). This work was partially carried out at the USTC Center for Micro and Nanoscale Research and Fabrication.

See Supplement 1 for supporting content.

[†]These authors contributed equally to this work.

REFERENCES

1. A. Cabello, S. Severini, and A. Winter, "Graph-theoretic approach to quantum correlations," Phys. Rev. Lett. **112**, 040401 (2014).
2. J. S. Bell, "On the problem of hidden variables in quantum mechanics," Rev. Mod. Phys. **38**, 447–452 (1966).
3. S. Kochen and E. P. Specker, "The problem of hidden variables in quantum mechanics," J. Math. Mech. **17**, 59–87 (1967).
4. C. Heunen, T. Fritz, and M. L. Reyes, "Quantum theory realizes all joint measurability graphs," Phys. Rev. A **89**, 032121 (2014).
5. R. Kunjwal, C. Heunen, and T. Fritz, "Quantum realization of arbitrary joint measurability structures," Phys. Rev. A **89**, 052126 (2014).
6. B. Bollobás, "The independence ratio of regular graphs," Proc. Am. Math. Soc. **83**, 433–436 (1981).
7. N. de Silva, "Graph-theoretic strengths of contextuality," Phys. Rev. A **95**, 032108 (2017).
8. S. Abramsky and A. Brandenburger, "The sheaf-theoretic structure of non-locality and contextuality," New J. Phys. **13**, 113036 (2011).
9. M. Grötschel, "Relaxations of vertex packing," J. Comb. Theory B **40**, 330–343 (1986).
10. L. Lovász, "On the Shannon capacity of a graph," IEEE Trans. Inf. Theory **25**, 1–7 (1979).
11. A. Acín, T. Fritz, A. Leverrier, and A. B. Sainz, "A combinatorial approach to nonlocality and contextuality," Commun. Math. Phys. **334**, 533–628 (2015).
12. A. Cabello, "Simple explanation of the quantum violation of a fundamental inequality," Phys. Rev. Lett. **110**, 060402 (2013).
13. B. Yan, "Quantum correlations are tightly bound by the exclusivity principle," Phys. Rev. Lett. **110**, 260406 (2013).
14. T. Fritz, A. B. Sainz, R. Augusiak, J. B. Brask, R. Chaves, A. Leverrier, and A. Acín, "Local orthogonality as a multipartite principle for quantum correlations," Nat. Commun. **4**, 2263 (2013).
15. M. Howard, J. Wallman, V. Veitch, and J. Emerson, "Contextuality supplies the 'magic' for quantum computation," Nature **510**, 351–355 (2014).
16. E. T. Campbell, "Enhanced fault-tolerant quantum computation in d-level systems," Phys. Rev. Lett. **113**, 230501 (2014).
17. N. Delfosse, P. A. Guerin, J. Bian, and R. Raussendorf, "Wigner function negativity and contextuality in quantum computation on rebits," Phys. Rev. X **5**, 021003 (2015).
18. M. Howard and E. Campbell, "Application of a resource theory for magic states to fault-tolerant quantum computing," Phys. Rev. Lett. **118**, 090501 (2017).
19. E. Nagali, V. D'Ambrosio, F. Sciarrino, and A. Cabello, "Experimental observation of impossible-to-beat quantum advantage on a hybrid photonic system," Phys. Rev. Lett. **108**, 090501 (2012).
20. E. Amselem, L. E. Danielsen, A. J. López-Tarrida, J. R. Portillo, M. Bourennane, and A. Cabello, "Experimental fully contextual correlations," Phys. Rev. Lett. **108**, 200405 (2012).
21. S. Yu and C. H. Oh, "State-independent proof of Kochen-Specker theorem with 13 rays," Phys. Rev. Lett. **108**, 030402 (2012).
22. B. Amaral, M. T. Cunha, and A. Cabello, "Quantum theory allows for absolute maximal contextuality," Phys. Rev. A **92**, 062125 (2015).
23. Z. P. Xu, H. Y. Su, and J. L. Chen, "Quantum contextuality of a qutrit state," Phys. Rev. A **92**, 012104 (2015).
24. R. Kunjwal and R. W. Spekkens, "From the Kochen-Specker theorem to noncontextuality inequalities without assuming determinism," Phys. Rev. Lett. **115**, 110403 (2015).
25. G. Cañas, E. Acuña, J. Cariñe, J. F. Barra, E. S. Gómez, G. B. Xavier, G. Lima, and A. Cabello, "Experimental demonstration of the connection between quantum contextuality and graph theory," Phys. Rev. A **94**, 012337 (2016).
26. A. Cabello, "Simple method for experimentally testing any form of quantum contextuality," Phys. Rev. A **93**, 032102 (2016).
27. A. Cabello, J. M. Estebaranz, and G. Garcia-Alcaine, "Bell-Kochen-Specker theorem: a proof with 18 vectors," Phys. Lett. A **212**, 183–187 (1996).
28. G. Kirchmair, F. Zähringer, R. Gerritsma, M. Kleinmann, O. Gühne, A. Cabello, R. Blatt, and C. F. Roos, "State-independent experimental test of quantum contextuality," Nature **460**, 494–497 (2009).
29. S. Castelletto, B. C. Johnson, V. Ivády, N. Stavrias, T. Umeda, A. Gali, and T. Ohshima, "A silicon carbide room-temperature single-photon source," Nat. Mater. **13**, 151–156 (2014).
30. A. A. Klyachko, M. A. Can, S. Binicioğlu, and A. S. Shumovsky, "Simple test for hidden variables in spin-1 systems," Phys. Rev. Lett. **101**, 020403 (2008).
31. R. Lapkiewicz, P. Li, C. Schaeff, N. K. Langford, S. Ramelow, M. Wieśniak, and A. Zeilinger, "Experimental non-classicality of an indivisible quantum system," Nature **474**, 490–493 (2011).